

Phase-resolved Spin Wave Tomography

Yusuke Hashimoto,¹ Tom H. Johansen,^{2,3} and Eiji Saitoh^{1,4,5}

¹*Advanced Institute for Materials Research, Tohoku University, Sendai 980-8577, Japan*

²*Department of Physics, University of Oslo, 0316 Oslo, Norway*

³*Institute for Superconducting and Electronic Materials,*

University of Wollongong, Northfields Avenue, Wollongong, NSW 2522, Australia

⁴*Institute for Materials Research, Tohoku University, Sendai 980-8577, Japan*

⁵*Advanced Science Research Center, Japan Atomic Energy Agency, Tokai 319-1195, Japan*

(Dated: May 8, 2022)

Propagation of spin waves in a magnetic medium has been discussed in terms of a dispersion relation of the spin waves. Recently, we developed a method, called spin wave tomography (SWaT), to obtain dispersion relation of spin waves in the long wavelength regime, so-called pure magnetostatic waves. In our previous paper on SWaT, phase information of spin waves was disregarded. In this report, we show advanced SWaT analysis, called phase-resolved spin wave tomography (PSWaT), to realize the direct observation of amplitude and phase of spin-wave propagation. The PSWaT is obtained by separating the real and the imaginary components of the complex Fourier transform in the SWaT analysis. We demonstrate PSWaT for spin waves excited by the photo-induced demagnetization in a Bi-doped garnet film, reflecting characteristic features of the complex dynamical susceptibility affected by magnetostatic coupling in the film.

A spin wave is a collective excitation of spin precessions in coupled spin systems. A phase shift between one spin to another is determined by the wavevector of a spin wave [1–4]. In spintronics and magnonics devices, data may be transferred by spin waves [5], so that its manipulation would be one of cornerstones for the development of spin-wave based applications [6].

The phase-resolved observation of spin waves has been realized with a Mach-Zehnder interferometer [1, 7], phase-sensitive Raman light scattering (PS-BLS) [8–10], and time-resolved magneto-optical (TRMO) spectroscopy [11–17]. Nowadays, the phase-resolved imaging of the propagation dynamics of optically-excited spin waves with sub-picosecond time resolution and micrometer spatial resolution has been realized with the TRMO method [18–27].

Recently, we have developed spin-wave tomography (SWaT): reconstruction of dispersion relation of spin waves [24]. The SWaT is based on the convolution theory, Fourier transform, and a pump-and-probe magneto-optical imaging method for spin-wave propagation. In the SWaT, the phase information of spin waves was lost due to the limitation in the data analysis procedure.

In this study, we demonstrate the reconstruction of dispersion relation of spin waves with their phase information by developing phase-resolved SWaT (PSWaT). The phase of a spin wave is determined with an advanced analysis procedure separating the real and the imaginary components of the complex Fourier transform in the SWaT analysis. The phase of the PSWaT spectra represents the complex dynamical susceptibility (χ) and the spatial symmetry of spin waves. Moreover, PSWaT provides information about the temporal evolution and the orientation of the torque generating the spin waves, exerted on the local magnetization (\mathbf{M}). Therefore, PSWaT allows us to investigate the characteristics and the excitation mechanism of spin waves.

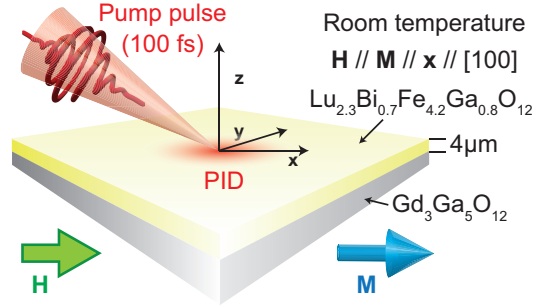


FIG. 1. Schematic illustration of the experimental configuration and the rectangular coordinate (x, y, z) used in this study. The sample surface is in the x - y plane with the x -axis along the orientation of \mathbf{M} parallel to the [100] axis. The orientation of \mathbf{M} was controlled by an external magnetic field (\mathbf{H}). The direction normal to the sample surface is along the z -axis. The pump pulse is focused on the sample surface at the origin of the coordinate and induces a photo-induced demagnetization (PID), which is the source of the spin waves investigated in this study.

The rectangular coordinate (x, y, z) shown schematically in Fig. 1 is used in this report. The sample surface is in the x - y plane with the x -axis parallel to the orientation of \mathbf{M} . The z -axis is along the sample normal. In our experiments, the pump and probe pulses illuminate the sample along the z -axis. The propagation dynamics of the optically-excited spin waves in the x - y plane ($m(\mathbf{r}, t)$) is observed with a magneto-optical imaging system (Fig. 2(a)) [28].

We consider spin waves in an in-plane magnetized garnet film excited by a photo-induced effective field $\mathbf{h}(\mathbf{r}, t) = h_z(\mathbf{r}, t) + ih_y(\mathbf{r}, t)$, where h_z and h_y are the fields along the z - and y -axes, respectively. The sample magnetization was controlled by applying an in-plane magnetic field, \mathbf{H} , with the intensity H_0 . We assume $H_0 \gg h_x, h_y$

so that the precession angle of \mathbf{M} is small. We consider a magnetic medium that has a translational invariance in the x - y plane. Then, the propagation dynamics of the spin waves is represented by the complex dynamical susceptibility $\chi(\mathbf{r}, t)$, or its Fourier transform (FT) $\chi(\mathbf{k}, \omega)$ [29].

The PSWaT is obtained by analyzing the propagation dynamics of the spin waves $\mathbf{m}(\mathbf{r}, t)$ excited by the photo-induced torque $\mathbf{h}(\mathbf{r}, t)$. Then, $\mathbf{m}(\mathbf{r}, t)$ is given by

$$\mathbf{m}(\mathbf{r}, t) = \int \int \int \chi(\mathbf{r} - \mathbf{a}, t - \tau) \mathbf{h}(\mathbf{a}, \tau) d\mathbf{a} d\tau. \quad (1)$$

According to the convolution theory, the FT of $\mathbf{m}(\mathbf{r}, t)$ is written as

$$\begin{aligned} \mathbf{m}(\mathbf{k}, \omega) &= \int \int \int \mathbf{m}(\mathbf{r}, t) \exp^{-i(\mathbf{k}\cdot\mathbf{r} - \omega t)} d\mathbf{r} dt \quad (2) \\ &= \chi(\mathbf{k}, \omega) \mathbf{h}(\mathbf{k}, \omega), \quad (3) \end{aligned}$$

where $\mathbf{m}(\mathbf{k}, \omega)$ and $\mathbf{h}(\mathbf{k}, \omega)$ are the FT of $\mathbf{m}(\mathbf{r}, t)$ and $\mathbf{h}(\mathbf{r}, t)$, respectively. When the z -component of \mathbf{m} (m_z) is observed through a Faraday effect, the SWaT intensity spectrum $|m_z(\mathbf{k}, \omega)|$ is obtained [24]. On the other hand, PSWaT described in the present paper deals with the phase information of spin waves by separating the real and the imaginary components of the FT spectra in the calculation of $m_z(\mathbf{k}, \omega)$.

The PSWaT spectra are obtained by applying the three-dimensional FT, composed of the time-space FT for the experimentally observed $m(\mathbf{r}, t)$, as shown schematically in Fig. 2(b). We here define the PSWaT spectra m_{pqs} , where p , q , and s label the real (r) and imaginary (i) components of the FT along the x -, y -, and time axes, respectively.

Let us first consider the spacial component of FT in the PSWaT analysis. For simplicity, we start from the one-dimensional FT for $m(x)$ with real values. $m(x)$ is decomposed into even ($m_e(x)$) and odd ($m_o(x)$) components, and we write

$$m(x) = m_e(x) + m_o(x). \quad (4)$$

Then, the FT of $m(x)$ along the x -axis (\mathcal{F}_x) is given by

$$\mathcal{F}_x\{m(x)\} = m(k_x) = m_r(k_x) + m_i(k_x) \quad (5)$$

with

$$m_r(k_x) = \mathcal{R}\{m(k_x)\} = \mathcal{F}_x\{m_e(x)\}, \quad (6)$$

$$m_i(k_x) = \mathcal{I}\{m(k_x)\} = \mathcal{F}_x\{m_o(x)\}, \quad (7)$$

where \mathcal{R} and \mathcal{I} are the real and the imaginary components, respectively [30]. Similarly, any two-dimensional data $m(x, y)$ is decomposed into four components with different symmetries as

$$m = m_{ee} + m_{eo} + m_{oe} + m_{oo}. \quad (8)$$

m_{ee} (m_{oo}) is a component with even (odd) symmetry along both x - and y -axes, while m_{eo} (m_{oe}) is a component with even (odd) symmetry along the x -(y)-axis and odd

(even) symmetry along the y -(x)-axis. The notation of (\mathbf{r}) is omitted for clarity. Then, the FT of m along the x - y plane (\mathcal{F}_{xy}) gives

$$\mathcal{F}_{xy}\{m(\mathbf{r})\} = m_{rr}(\mathbf{k}) + m_{ri}(\mathbf{k}) + m_{ir}(\mathbf{k}) + m_{ii}(\mathbf{k}) \quad (9)$$

with $m_{rr}(\mathbf{k}) = \mathcal{F}_{xy}\{m_{ee}(\mathbf{r})\}$, $m_{ri}(\mathbf{k}) = \mathcal{F}_{xy}\{m_{eo}(\mathbf{r})\}$, $m_{ir}(\mathbf{k}) = \mathcal{F}_{xy}\{m_{oe}(\mathbf{r})\}$, and $m_{ii}(\mathbf{k}) = \mathcal{F}_{xy}\{m_{oo}(\mathbf{r})\}$. Therefore, the complex components obtained by the spacial FT represent the spatial symmetry of the observed spin waves.

Finally, the PSWaT spectra are obtained by applying the temporal FT (\mathcal{F}_t) to the four components of the m_{rr} , m_{ir} , m_{ri} , and m_{ii} . We write

$$m_{pqr}(\mathbf{k}, \omega) = \mathcal{R}\{\mathcal{F}_t\{m_{pq}(\mathbf{k}, t)\}\}, \quad (10)$$

$$m_{pqi}(\mathbf{k}, \omega) = \mathcal{I}\{\mathcal{F}_t\{m_{pq}(\mathbf{k}, t)\}\}. \quad (11)$$

We define the phase of the PSWaT spectra for the temporal FT as $\phi_{pq}(\mathbf{k}, \omega) = \tan^{-1}[m_{pqi}(\mathbf{k}, \omega)/m_{pqr}(\mathbf{k}, \omega)]$. This represents the initial phase of the spin waves with $m(\mathbf{k}, \omega) \propto \exp\{i\phi_{pq}(\mathbf{k}, \omega)\}$. This is the basic concept of PSWaT.

We examine SWaT and PSWaT for a 4- μm thick $\text{Lu}_{2.3}\text{Bi}_{0.7}\text{Fe}_{4.2}\text{Ga}_{0.8}\text{O}_{12}$ film grown on a $\text{Gd}_3\text{Ga}_5\text{O}_{12}$ (001) substrate. The sample is in-plane magnetized with the saturation magnetization of 780 Oe, which was measured with a vibrating sample magnetometer. The orientation of the \mathbf{M} was controlled by applying an external magnetic field of 560 Oe along the [100] axis.

The SWaT and PSWaT spectra are obtained by analyzing propagation dynamics of optically-excited spin waves, observed with a time-resolved magneto-optical imaging method (Fig. 2(a)) [20]. We used a pulsed light source with 100 fs time duration and a repetition frequency of 1 kHz. This beam was divided into two beams: pump and probe. The pump beam was focused on the sample surface by an objective with the radius of 2 μm . The excited spin waves were observed with the probe beam, which was weakly focused on the sample surface with the radius of 1 mm. The wavelength of the probe beam was changed with an optical parametric amplifier to 630 nm, where the sample shows a large Faraday rotation angle (5.2 degree) and high transmissivity (41 %). The fluence of the pump and the probe beams were 1.2 J cm^{-2} and 0.2 mJ cm^{-2} , respectively. The propagation dynamics of the spin waves was observed with a magneto-optical imaging system based on a rotation analyzer method using a CCD camera [20]. The spatial resolution of the system is a micrometer, given by the diffraction limit of the probe beam. All the experiments were performed at room temperature. The detail of the experimental setup was summarized in Ref. 20.

Let us first show SWaT spectra under the in-plane magnetic field of 560 Oe, where the spin waves are mainly excited by the PID [24]. The illumination of a magnetic medium with an intense pump pulse decreases local magnetization [20]. This change in local magnetization ($\delta\mathbf{m}(\mathbf{r})$) induces an extra demagnetization field ($\mathbf{h}_y^{\text{PID}}(\mathbf{r})$) in the surrounding area and generates spin

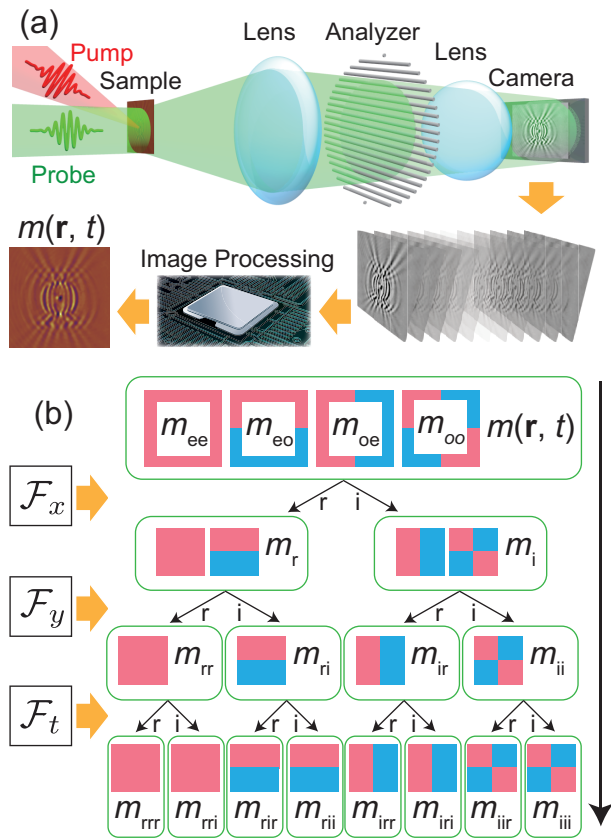


FIG. 2. (a) Schematic illustration of the experimental setup. The propagation dynamics of the optically-excited spin waves ($m(\mathbf{r}, t)$) is observed with a system based on a pump-and-probe technique and a rotation analyzer method. The time delay between the pump and probe pulses is controlled by a mobile stage. All the data obtained by the CCD camera are transferred to a processor to obtain magneto-optical images of $m(\mathbf{r}, t)$. (b) The PSWaT spectra are obtained by analyzing the $m(\mathbf{r}, t)$ data with the three-dimensional FT along the x-axis (\mathcal{F}_x), y-axis (\mathcal{F}_y), and time-axis (\mathcal{F}_t). The real (r) and imaginary components of the complex FT spectra are separated.

waves [14, 19, 32]. The demagnetization field lasts long time, and we write $\mathbf{h}_y^{\text{PID}}(\mathbf{r}, t) = \mathbf{h}_y^{\text{PID}}(\mathbf{r})\Theta(t)$, where $\Theta(t)$ is the Heaviside step function. Then, the PSWaT spectrum for $\omega \neq 0$ is

$$\mathbf{m}^{\text{PID}}(\mathbf{k}, \omega) = -\frac{\mathbf{h}_y^{\text{PID}}(\mathbf{k})}{\omega} \chi(\mathbf{k}, \omega). \quad (12)$$

Figure 3(a) shows the angular dependence of the SWaT spectra along various \mathbf{k} directions [24]. We see branches caused by the spin waves in the frequency range from 2 GHz to 3 GHz. A dispersion relation of the spin waves is read. The white dashed lines in Fig. 3(a) are the fitting results with the Damon-Eshbach theory [31], representing the dispersion relation of magnetostatic waves. By using the parameters obtained, the dispersion relation of the magnetostatic spin waves is reconstructed as shown in Fig. 3(b). The anisotropic nature of the dispersion

relation is due to that of the dipolar coupling [3, 24, 31].

Next, we show the PSWaT spectra in Fig. 4. Since $\mathbf{h}_y^{\text{PID}}(\mathbf{r})$ has mirror symmetry for both x and y axes as schematically drawn in Fig. 4(a), the excited spin waves appear in the m_{ii} component. Figures 4(b) and 4(c) show the m_{iir} and m_{iii} components of the PSWaT spectra along the direction of $\phi = 32$ degree, where ϕ is the angle between \mathbf{M} and \mathbf{k} . We see branches with different features in the m_{iir} and m_{iii} components. Figures 4(d) and 4(e) show the cross-section of the PSWaT spectra shown in Figs. 4(b) and 4(c), respectively, at $k = 1.0 \times 10^4$ rad cm^{-1} . We see dispersion-type and absorption-type spectra in the m_{iir} and m_{iii} components, respectively. These features are well explained by a Landau-Lifshitz-Gilbert (LLG) equation

$$\frac{d\mathbf{M}}{dt} = -\gamma\mu_0(\mathbf{M} \times \mathbf{H}_{\text{eff}}) + \frac{\alpha}{M_s}(\mathbf{M} \times \frac{d\mathbf{M}}{dt}), \quad (13)$$

where \mathbf{H}_{eff} is the total effective field, γ is the gyromagnetic ratio, μ_0 is the magnetic permeability of free space, and α is the Gilbert damping constant. By solving the LLG equation [3], we obtain $\chi(\mathbf{k}, \omega) = \chi(\mathbf{k}, \omega) + i\kappa(\mathbf{k}, \omega)$ with

$$\chi(\mathbf{k}, \omega) = \frac{\omega_0(\mathbf{k}) \pm \omega}{(\omega_0(\mathbf{k}) \pm \omega)^2 + \alpha^2\omega^2} \quad (14)$$

and

$$\kappa(\mathbf{k}, \omega) = \frac{\alpha\omega}{(\omega_0(\mathbf{k}) - \omega)^2 + \alpha^2\omega^2}, \quad (15)$$

where $\omega_0(\mathbf{k})$ represents the dispersion relation of the spin waves. The χ and κ well reproduce the observed m_{iir} and m_{iii} PSWaT spectra with the parameters of $\omega_0(\mathbf{k})/2\pi = 2.56$ GHz and $\alpha = 0.03$, respectively, as shown by the dashed curves in Figs. 4(d) and 4(e). In the present case, the maximum time-delay between the pump and probe pulses ($T_{\text{max}} = 13$ ns) is much shorter than the spin relaxation time of the present sample, so that α is limited by the T_{max} giving $\alpha \sim 2\pi/(\omega T_{\text{max}}) = 0.03$.

In summary, we developed phase-resolved spin wave tomography (PSWaT) to obtain spin-wave dispersion with phase information. The PSWaT is based on the convolution theory, Fourier transform, and a time-resolved magneto-optical imaging method. The PSWaT analysis separates the real and the imaginary components of the complex Fourier transform in the spin wave tomography (SWaT) [24]. The PSWaT was examined by using a Bi-doped in-plane magnetized garnet film. The PSWaT spectra for spin waves generated by a photo-induced demagnetization are well explained by a calculation based on the LLG equation.

ACKNOWLEDGMENTS

We thank Dr. R. Iguchi for fruitful discussions. This work was financially supported by JST-ERATO

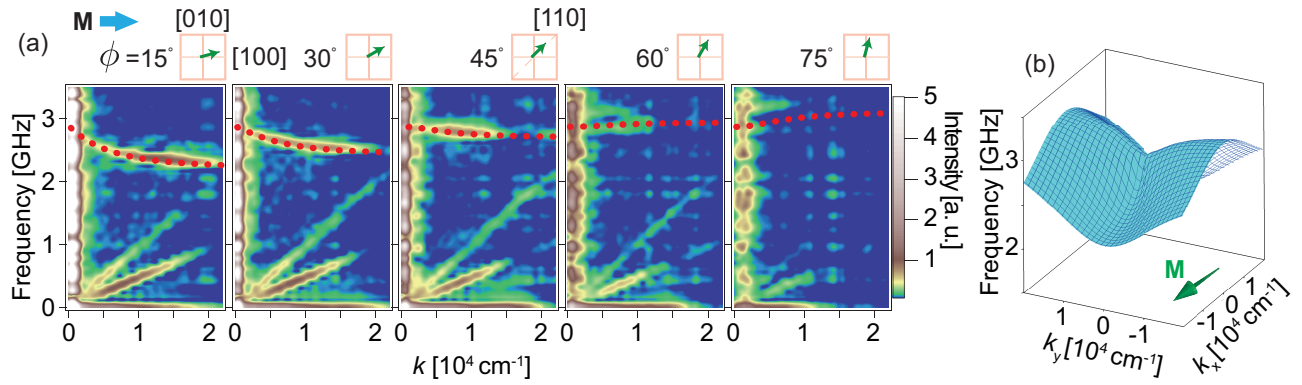


FIG. 3. (a) The angular dependence of the SWaT spectra for various \mathbf{k} directions with an angle (ϕ) between \mathbf{M} and \mathbf{k} . The red dotted lines are the dispersion relation of the volume mode of the magnetostatic spin waves calculated with the Damon-Eshbach theory [31]. (b) The dispersion relation of the volume mode of the magnetostatic spin waves calculated with the parameters obtained.

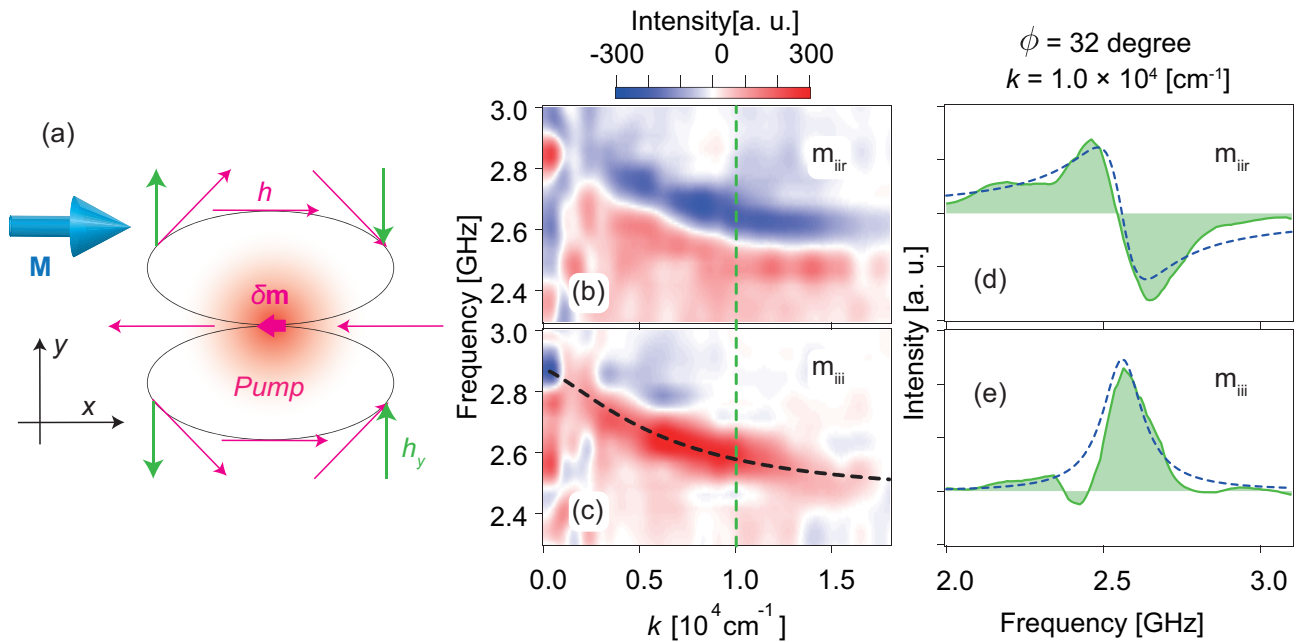


FIG. 4. (a) Schematic illustration of the field induced by the photo-induced demagnetization ($\delta\mathbf{m}$). The field along the y -axis (h_y) generates spin waves with mirror symmetries about both the x - and y -axes. The m_{iir} (b) and m_{iii} (c) components of the PSWaT spectra along the direction of $\phi = 32$ degree. An in-plane magnetic field of 560 Oe was applied along the [100] axis. The black dashed line in (c) is the dispersion relation of the magnetostatic waves calculated with the Damon-Eshbach model [31]. Figures (d) and (e) are the cross-sections of the data shown in (b) and (c) along $k = 1.0 \times 10^4 \text{ cm}^{-1}$ (green dashed lines in (b) and (c)). The dashed lines in (d) and (e) are calculated with Eqs. 14 and 15, respectively, with $\omega_0(\mathbf{k})/2\pi = 2.56$ GHz and $\alpha = 0.03$.

Grant Number JPMJER1402, and World Premier In-

ternational Research Center Initiative (WPI), all from MEXT, Japan.

- [1] T. Schneider, A. A. Serga, B. Leven, B. Hillebrands, R. L. Stamps, and M. P. Kostylev, *Applied Physics Letters* **92**, 022505 (2008).
 [2] K. S. Lee and S. K. Kim, *Journal of Applied Physics* **104**,

053909 (2008).

- [3] D. D. Stancil and A. Prabhakar, *Spin Waves, Theory and Applications* (Springer Science & Business Media, 2009).
 [4] A. A. Serga, A. V. Chumak, and B. Hillebrands, *Journal*

- of Physics D-Applied Physics **43**, 264002 (2010).
- [5] A. V. Chumak, V. I. Vasyuchka, A. A. Serga, and B. Hillebrands, *Nature Physics* **11**, 453 (2015).
- [6] A. Khitun, M. Bao, and K. L. Wang, *IEEE Transactions on Magnetics* **44**, 2141 (2008).
- [7] M. P. Kostylev, A. A. Serga, T. Schneider, B. Leven, and B. Hillebrands, *Applied Physics Letters* **87**, 153501 (2005).
- [8] L. Fallarino, M. Madami, G. Duerr, D. Grundler, G. Gubbiotti, S. Tacchi, and G. Carlotti, *IEEE Transactions on Magnetics* **49**, 1033 (2013).
- [9] F. Fohr, A. A. Serga, T. Schneider, J. Hamrle, and B. Hillebrands, *Review of Scientific Instruments* **80** (2009).
- [10] A. A. Serga, T. Schneider, B. Hillebrands, S. O. Demokritov, and M. P. Kostylev, *Applied Physics Letters* **89**, 063506 (2006).
- [11] S. A. Crooker, J. J. Baumberg, F. Flack, N. Samarth, and D. D. Awschalom, *Physical Review Letters* **77**, 2814 (1996).
- [12] A. Kirilyuk, A. V. Kimel, and T. Rasing, *Reviews of Modern Physics* **82**, 2731 (2010).
- [13] E. Carpene, E. Mancini, C. Dallera, E. Puppini, and S. De Silvestri, *Thin Solid Films* **519**, 1642 (2010).
- [14] B. Lenk, H. Ulrichs, F. Garbs, and M. Münzenberg, *Physics Reports* **507**, 107 (2011).
- [15] D. Bossini, S. Dal Conte, Y. Hashimoto, A. Secchi, R. V. Pisarev, T. Rasing, G. Cerullo, and A. V. Kimel, *Nature Communications* **7**, 10645 (2016).
- [16] J. Janusonis, C. L. Chang, T. Jansma, A. Gatilova, V. S. Vlasov, A. M. Lomonosov, V. V. Temnov, and R. I. Tobey, *Physical Review B* **94**, 024415 (2016).
- [17] D. Bossini and T. Rasing, *Physica Scripta* **92**, 024002 (2017).
- [18] T. Satoh, Y. Terui, R. Moriya, B. A. Ivanov, K. Ando, E. Saitoh, T. Shimura, and K. Kuroda, *Nature Photonics* **6**, 662 (2012).
- [19] Y. Au, M. Dvornik, T. Davison, E. Ahmad, P. S. Keatley, A. Vansteenkiste, B. Van Waeyenberge, and V. V. Kruglyak, *Physical Review Letters* **110**, 097201 (2013).
- [20] Y. Hashimoto, A. R. Khorsand, M. Savoini, B. Koene, D. Bossini, A. Tsukamoto, A. Itoh, Y. Ohtsuka, K. Aoshima, A. V. Kimel, A. Kirilyuk, and T. Rasing, *Review of Scientific Instruments* **85**, 063702 (2014).
- [21] I. Yoshimine, T. Satoh, R. Iida, A. Stupakiewicz, A. Maziewski, and T. Shimura, *Journal of Applied Physics* **116**, 043907 (2014).
- [22] N. Ogawa, W. Koshibae, A. J. Beekman, N. Nagaosa, M. Kubota, M. Kawasaki, and Y. Tokura, *Proceedings of the National Academy of Sciences* **112**, 8977 (2015).
- [23] S. Iihama, Y. Sasaki, A. Sugihara, A. Kamimaki, Y. Ando, and S. Mizukami, *Physical Review B* **94**, 020401(R) (2016).
- [24] Y. Hashimoto, S. Daimon, R. Iguchi, Y. Oikawa, K. Shen, K. Sato, D. Bossini, Y. Tabuchi, T. Satoh, B. Hillebrands, G. E. W. Bauer, T. H. Johansen, A. Kirilyuk, T. Rasing, and E. Saitoh, *Nature Communications* **8**, 15859 (2017).
- [25] Y. Hashimoto, D. Bossini, T. H. Johansen, E. Saitoh, A. Kirilyuk, and T. Rasing, *arxiv.org*, arXiv:1710.08087.
- [26] A. Kamimaki, S. Iihama, Y. Sasaki, Y. Ando, and S. Mizukami, *Physical Review B* **96**, 014438 (2017).
- [27] I. V. Savochkin, M. Jäckl, V. I. Belotelov, I. A. Akimov, M. A. Kozhaev, D. A. Sylgacheva, A. I. Chernov, A. N. Shaposhnikov, A. R. Prokopov, V. N. Berzhansky, D. R. Yakovlev, A. K. Zvezdin, and M. Bayer, *Scientific Reports* **7**, 391002 (2017).
- [28] A. K. Zvezdin and V. A. Kotov, *Modern Magnetooptics and Magneto-optical Materials* (CRC Press, 1997).
- [29] R. M. White, *Quantum Theory of Magnetism*, *Magnetic Properties of Materials*, Vol. 32 (Springer Science & Business Media, Berlin, Heidelberg, 2013).
- [30] R. M. Gray and J. Goodman, *Fourier Transforms*, *An Introduction for Engineers* (Springer Science & Business Media, 2012).
- [31] M. J. Hurben and C. E. Patton, *Journal of Magnetism and Magnetic Materials* **139**, 263 (1995).
- [32] M. van Kampen, C. Jozsa, J. T. Kohlhepp, P. LeClair, L. Lagae, W. J. M. de Jonge, and B. Koopmans, *Physical Review Letters* **88**, 227201 (2002).